



**CHALMERS**  
UNIVERSITY OF TECHNOLOGY

---

# **Calibrating Inherent Strain for Additive Manufacturing**

An investigation of different subscale geometries

Master's thesis in Product Development

KOUSHIK RAVICHANDRAN



MASTER'S THESIS IN PRODUCT DEVELOPMENT

# Calibrating Inherent Strain for Additive Manufacturing

An investigation of different subscale geometries

KOUSHIK RAVICHANDRAN



Department of Industrial and Materials Science  
CHALMERS UNIVERSITY OF TECHNOLOGY  
Göteborg, Sweden 2020.

**Calibrating Inherent Strain for Additive Manufacturing**  
An investigation of different subscale geometries

KOUSHIK RAVICHANDRAN

© KOUSHIK RAVICHANDRAN, 2020.

Supervisor: Joel Larsson, GKN Aerospace Sweden AB  
Examiner: Gauti Asbjörnsson, Department of Industrial and Material Science  
Chalmers Supervisor: Simon Grunditz, Department of Industrial and Materials Science

Master's Thesis 2020:NN  
Department of Industrial and Materials Science  
Chalmers University of Technology  
SE-412 96 Göteborg  
Sweden  
Telephone: + 46 (0)31-772 1000

Printed by Chalmers Reproservice  
Göteborg, Sweden 2020.

## **Calibrating Inherent Strain for Additive Manufacturing**

Master's thesis Product Development

KOUSHIK RAVICHANDRAN

Department of Industrial and Materials Science

Chalmers University of Technology

## **Abstract**

Additive manufacturing (AM) is gaining popularity over the years and process simulation has become a crucial step to effectively assess the AM process. Due to the high temperature gradients, residual stress and deformation that resides in the final product, predicting residual stress, and deformation during simulation is a crucial step to estimate the producibility of the geometry. This thesis work aims to identify whether the modified inherent strain method can replace the computationally costly thermo-mechanical simulation method to assess the deformation for the deposition of material onto large scale geometries.

In this thesis, a multi-scale approach is used to establish a workflow for the inherent strain method where two different scales of models are used for the simulation, i.e., a sub-scale model and a large-scale model. The thesis aims to study the geometric influence of the sub-scale model for prediction and calibration of the inherent strain tensors with respect to deformation. In this study, eight different subscale models with different configurations were simulated and calibrated. The calibrated inherent strain tensors of the subscale model were compared with the sensitivity analysis of the large-scale model to identify the best fit sub-scale model, taking the first step towards establishing a viable workflow for the inherent strain.

Keywords: Additive Manufacturing, Process simulation, Inherent strain method.



# Acknowledgments

Firstly, I would like to thank Chalmers University of Technology and GKN Aerospace Sweden AB for giving me the opportunity to be part of a master thesis project. I would like to express my sincere gratitude to my supervisors, Joel Larsson from the process simulation department, GKN Aerospace Sweden AB. Moreover I would like to thank my examiner Gauti Asbjörnsson, Assistant professor, division of Product development and Simon Grunditz PhD Student at the division of Product Development for their constant support and guidance throughout this journey.

I would like to thank the process simulation team at GKN Aerospace Sweden AB for their valuable suggestions and feedback throughout the thesis. At last, I would like to thank my family and friends for their constant support and care throughout this journey.

KOUSHIK RAVICHANDRAN, Gothenburg, September 2020

# Nomenclature

## Abbreviations

AM	Additive Manufacturing
CAD	Computer-Aided Design
DED	Direct Energy Deposition
LMD-w	Laser Metal Deposition-wire
FEA	Finite Element Analysis
TM	Thermo-mechanical
BC	Boundary Condition
HAZ	Heat Affected Zone
LMD	Laser Metal Deposition
LENS	Laser Engineered Net Shaping
EBAM	Electron Beam Additive Manufacturing
Al	Aluminium
C	Carbon
Fe	Iron
H	Hydrogen
N	Nitrogen
O	Oxygen
Ti	Titanium
V	Vanadium

## Symbols

$\varepsilon$	Strain
mm	Millimeter

# Contents

Abstract .....	V
Acknowledgments.....	VII
Nomenclature .....	VIII
<b>List of Figures.....</b>	<b>XI</b>
<b>List of Tables .....</b>	<b>XII</b>
<b>1 Introduction.....</b>	<b>1</b>
1.1 Project Background .....	1
1.2 GKN Aerospace .....	1
1.3 Aim:.....	2
1.4 Research Questions .....	2
1.5 Delimitations .....	2
<b>2 Theory .....</b>	<b>3</b>
2.1 Additive Manufacturing .....	3
2.2 AM Product development .....	3
2.3 Direct energy deposition (DED) .....	3
2.3.1 Laser metal deposition-wire (LMD-w):.....	5
2.4 Welding process .....	5
2.5 Strain .....	5
2.6 Finite element analysis .....	6
2.6.1 Thermo-mechanical analysis: .....	6
2.6.2 Original Inherent strain theory:.....	6
2.6.3 Modified theory Inherent strain .....	7
2.7 Sub structuring .....	8
2.8 Element birth and death technique .....	9
2.9 Calibration of inherent strain tensor .....	10
<b>3 Methodology .....</b>	<b>11</b>
3.1 Multi-scale approach .....	11
<b>4 Workflow .....</b>	<b>13</b>
4.1 CAD Models .....	13
4.1.1 Layer configuration.....	13
4.1.2 Geometric configuration .....	14
4.1.3 Weld path configuration .....	15
4.2 Material .....	16
4.3 Weld path .....	16
4.4 Meshing .....	17
4.5 Boundary Condition .....	17
4.6 Load cases .....	18

4.7	Calibration.....	19
4.8	Thermo-mechanical simulation.....	20
4.9	Inherent strain simulation.....	21
4.10	Sensitivity Analysis.....	21
<b>5</b>	<b>Results and Discussions.....</b>	<b>22</b>
5.1	Deformation Results.....	22
5.1.1	Layer Configuration.....	22
5.1.2	Geometric Configuration.....	22
5.1.3	Weld path configuration.....	23
5.2	Calibration Results.....	23
5.2.1	Layer configuration.....	24
5.2.2	Geometric configuration.....	24
5.2.3	Weld path configuration.....	26
5.3	Sensitivity analysis results.....	26
5.4	New Thermal Boundary condition (BC2).....	27
5.4.1	Deformation Results.....	27
5.4.2	Calibration Results.....	28
5.5	Time Evaluation.....	29
<b>6</b>	<b>Conclusion.....</b>	<b>30</b>
6.1	Conclusion.....	30
6.2	Future Work.....	30
	<b>References.....</b>	<b>32</b>

# List of Figures

Figure 2.1 AM Product development cycle. ....	3
Figure 2.2 DED process map .....	4
Figure 2.3 Powder feed AM process, (Mattsson, 2015) .....	4
Figure 2.4 Laser metal deposition-wire (LMD-w), (Hryha, 2019).....	5
Figure 2.5 Relation between stress and strain to determine the elastic strain and plastic strain.....	6
Figure 2.6 Overview of flow in a TM analysis, (Mattsson, 2015).....	6
Figure 2.7 Different states for the definition of the inherent strain undeformed state (left), stressed state (middle), and stress relived-state (right) (Xuan Liang L. C., 2018) .....	7
Figure 2.8 Inherent strain curve .....	8
Figure 2.9 Example of sub structuring.....	9
Figure 2.10 Element birth technique.....	9
Figure 2.11 Two-layer example for illustration of the layer-by-layer method of assigning the inherent strain (Xuan Liang Q. C., 2019). ....	10
Figure 3.1 Sub structuring of fan case (right) to subscale models (left).....	11
Figure 3.2 Flow chart of Multi-scale approach.....	12
Figure 4.1 M1- 17 layer of bead .....	13
Figure 4.2 M2- 29 layers of bead.....	14
Figure 4.3 M3- 10 layers of bead.....	14
Figure 4.4 M4- 16 layers of bead.....	14
Figure 4.5 M5- Two bead deposition.....	15
Figure 4.6 M6- Parallel weld path configuration.....	15
Figure 4.7 M7- Subsequent weld path configuration.....	16
Figure 4.8 Horizontal direction scanning strategy (Sonja Jonsson, 2018). ....	16
Figure 4.9 Visualizing of weld path, red crosses marks the weld paths and green dots marks the orientation paths (Forslund, 2018) .....	17
Figure 4.10 Mesh .....	17
Figure 4.11 Mechanical boundary condition .....	18
Figure 4.12 Schematic view of the thermal boundary condition BC1(left) and BC2(right).....	18
Figure 4.13 Load case for TM simulation .....	19
Figure 4.14 Load case for mechanical analysis .....	19
Figure 4.15 Deformation contribution vs number of layers .....	19
Figure 4.16 TM simulation .....	20
Figure 4.17 Nodes Sp1, Sp2, and Sp3 for extraction of target deformation.....	20
Figure 4.18 Inherent strain simulation setup.....	21
Figure 5.1 Deformation results for layer configuration M1, M2, and M3.....	22
Figure 5.2 Deformation results for geometric configuration M1 and M4 .....	23
Figure 5.3 Deformation results for weld path configuration M5 and M6 .....	23
Figure 5.4 Calibration results for layer configuration M1, M2 and M3 .....	24
Figure 5.5 Calibration results for geometric configuration M1 and M4.....	25
Figure 5.6 Calibration results for geometric configuration M5 and M7.....	25
Figure 5.7 Calibration results for geometric configuration M5 and M6.....	26
Figure 5.8 Sensitivity analysis error vs inherent strain tensor .....	27
Figure 5.9 Deformation results for M1 with thermal boundary condition BC2 .....	28
Figure 5.10 Calibration results for geometric configuration M1 and M1_BC2 .....	29

## List of Tables

Table 4.1 Ti64 material composition .....	16
Table 4.2 Calibrated inherent strain tensor .....	20
Table 4.3 Inherent strain tensor used in sensitivity analysis.....	21
Table 5.1 Calibrated inherent strain tensors for M1, M2, and M3 .....	24
Table 5.2 Calibrated inherent strain tensors for M1 and M4 .....	25
Table 5.3 Calibrated inherent strain tensors for M5 and M7 .....	26
Table 5.4 Calibrated inherent strain tensors for M5 and M6 .....	26
Table 5.5 Best fit inherent strain tensor from sensitivity analysis.....	27
Table 5.6 Calibrated inherent strain tensors for M1 and M1_BC2.....	28
Table 5.7 Time evaluation for the subscale model .....	29

# 1 Introduction

This chapter aims to introduce the reader to the project background, aim of the project, and research questions that are addressed in this thesis work, along with the delimitations and considerations.

## 1.1 Project Background

GKN Aerospace is currently focusing on the development of fast and accurate methods to simulate Additive Manufacturing (AM). Currently, in the AM product development cycle, experimental evaluation is carried out to understand the relationship between the final part/geometry and the process parameters. Experimental evaluations are expensive and time-consuming, also the output depends on other different parameters involved in the process. To ensure the manufacturability and quality of the product a faster and accurate way of predicting deformation is necessary. Numerical simulation seems to be a viable alternative solution by establishing the real process for different sets of process parameters (Matteo Bugatti, 2018). Predicting residual stress and deformation during simulation is a crucial step to estimate the producibility of geometry and the process parameters.

The foundation of AM simulation is welding simulation since the AM process involves welding the material layer-wise. Traditionally in AM simulation, Thermo-mechanical (TM) simulations are carried out to predict the deformation. Depending on the size and number of layers of the model the computational time ranges from days to weeks, or even months (Nils Keller, 2014).

The Inherent strain simulation is one such method used for predicting the deformation quickly in welding simulation. The process of AM is a series of welding passes in a controlled path flow, which is similar to the welding process. Thus, the theories and methods of welding simulation are applied to the AM process simulation. The original inherent strain theory is modified slightly for the AM process. The modified inherent strain methodology is used to minimize the need for the computationally costly TM simulation. In the modified inherent strain method, the transient weld heat source is replaced by the residual shrinkage to capture the final mechanical behavior caused by the thermal weld cycle.

To bypass the time consuming and costly TM simulation, a method/workflow is created to implement the modified inherent strain theory into practice for faster and accurate simulation results. By implementing this process, the product/component can be evaluated and validated in the design stage itself. Several studies have been done in the past concerning the implementation of the modified inherent strain method for AM simulation, considering different parameters such as scanning strategy, layer thickness, and other process parameters.

## 1.2 GKN Aerospace

This Master thesis has been carried out at GKN Aerospace Sweden AB, which produces engine components, aircraft structures, cabin windows and cabling for aircrafts. In Trollhättan, they develop and manufacture engine parts for aircraft, and space rockets.

### **1.3 Aim:**

The thesis aims to investigate the Inherent strain method and its application for the laser metal deposition-wire AM process. The primary aim of the thesis will focus on studying the influence of subscale geometry when calibrating the inherent strains. The thesis work will also focus on establishing a workflow for calibrating inherent strains to bypass the TM simulation for faster prediction of deformation in large-scale components in the aerospace industry.

### **1.4 Research Questions**

The scope of this thesis can be described by the following research questions:

- *RQ1: Can modified inherent strain simulation replace TM simulation for simulation of large components?*
- *RQ2: How should the sub-scale geometry be defined and how does it influence the prediction and calibration of inherent strains with respect to deformation?*
- *RQ3: Evaluate the time reduction between TM simulation and inherent strain method simulation?*

### **1.5 Delimitations**

In this master thesis, the method/workflow is developed only for laser metal deposition-wire additive manufacturing. The influence of scanning or hatching strategy is not studied in this work. The simulation results are not validated by experimental evaluation. A Fan case is used as a large-scale component and the methodology is developed to evaluate the deformation of that component alone. The calibrated inherent strain tensors are isotropic in nature.

## 2 Theory

This chapter aims at providing the reader with the relevant theories to perform this thesis work.

### 2.1 Additive Manufacturing

Additive manufacturing is gaining popularity over the years. In contrast to the traditional material removal technique, an unconventional material addition in an incremental manner is used in the AM process. Using the AM manufacturing technique, we can swiftly manufacture a component using the computer design model with high precision.

AM can be used to produce complex geometries with fewer materials waste and energy. The AM can be distinguished into seven process categories.

1. Vat photopolymerization
2. Powder bed fusion
3. Material extrusion
4. Material jetting
5. Binder jetting
6. Directed energy deposition
7. Sheet lamination

### 2.2 AM Product development

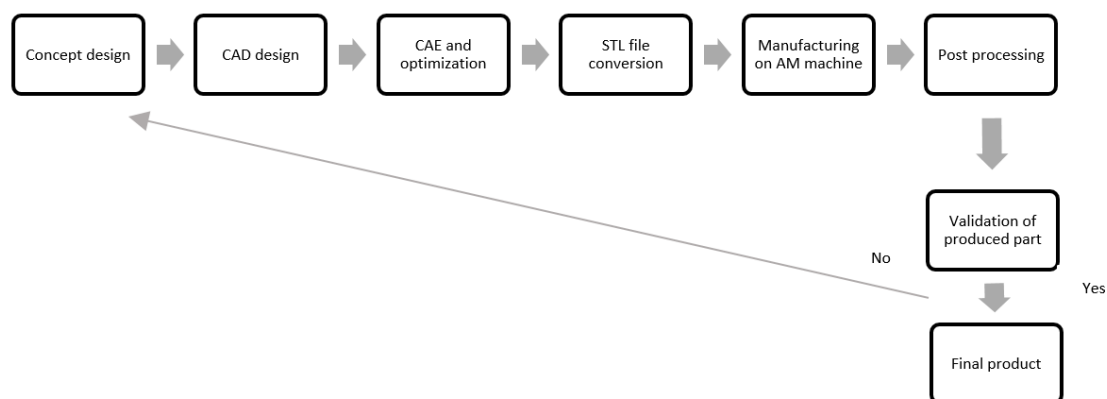


Figure 2.1 AM Product development cycle.

As stated in (Hryha, 2019) the AM product development cycle is shown in Figure.2.1. In the AM product development cycle the product is designed from a conceptual design phase. Then following the detailed design phase or Computer-aided design (CAD) phase; the designed geometry is further analyzed and optimized, and the optimized geometry is manufactured through the AM process. Once the part is manufactured, it undergoes post-processing treatments to improve its properties. Finally, the produced part is tested and evaluated to examine if the product fulfills the design requirement. If the part produced fails to meet the design requirement the entire AM product development cycle is repeated for the new concept or design.

### 2.3 Direct energy deposition (DED)

Direct energy deposition is a process of fusing the material by a heat source (laser or electron beam) as it is being deposited. Direct energy deposition is mostly used to repair

or rebuild additional material to the surface of the component. Several process categories working under the Directed energy deposition principle.

- Laser Metal Deposition (LMD)
- Laser Engineered Net Shaping (LENS)
- Electron Beam Additive Manufacturing (EBAM)
- Directed Light fabrication
- 3D laser Cladding

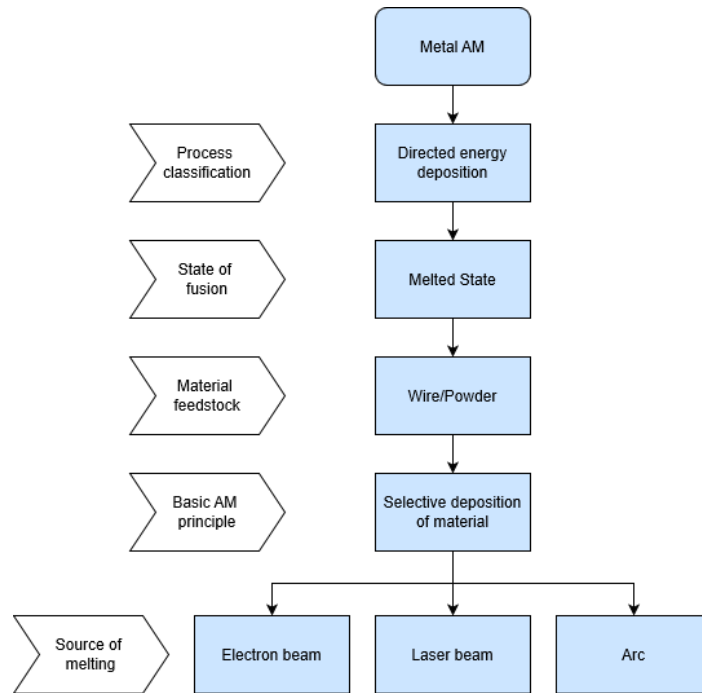


Figure 2.2 DED process map

The DED AM principle can be broadly classified based on the Material feedstock as:

- Powder blown system
- Wire-feed system

**Powder-blown system:** material powder is feed through a nozzle and melted by a laser beam on the surface of the component. The powder feed AM process is illustrated in Figure 2.3.

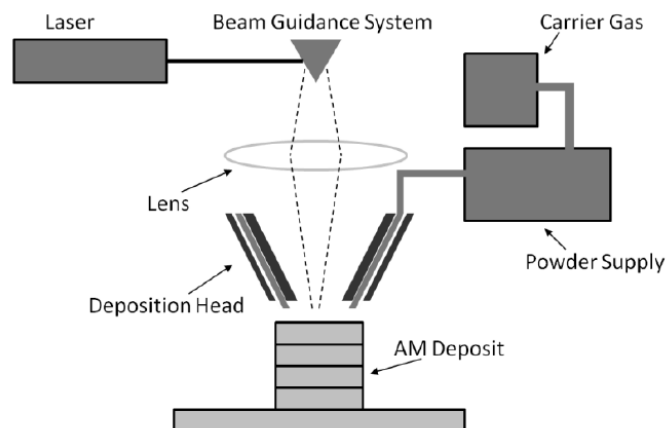


Figure 2.3 Powder feed AM process, (Mattsson, 2015)

**Wire-feed systems:** wire is feed through a nozzle and melted by a heat source (laser beam, electron beam, or a plasma arc) under protective gas or air, Figure 2.4.

### 2.3.1 Laser metal deposition-wire (LMD-w):

The laser power melts down the metal wire feed through a nozzle. Due to the process of solidification, a bead is formed in layers, and the layers can be welded in a single or multiple weld pass per layer. This process is numerically controlled by a controlling unit. The Advantages of LMD-w is that it can manufacture large geometries since it has a high deposition rate. The process involves a high cooling rate and low material wastage. In conclusion, wire feed direction, position, and welding parameters are some of the important parameters that need to be considered in producing large metal products without cracking and porosity (Donghong Ding, 2015). The drawbacks of LMD-w are that it has high residual stress and distortions due to excessive heat input and a high deposition rate.

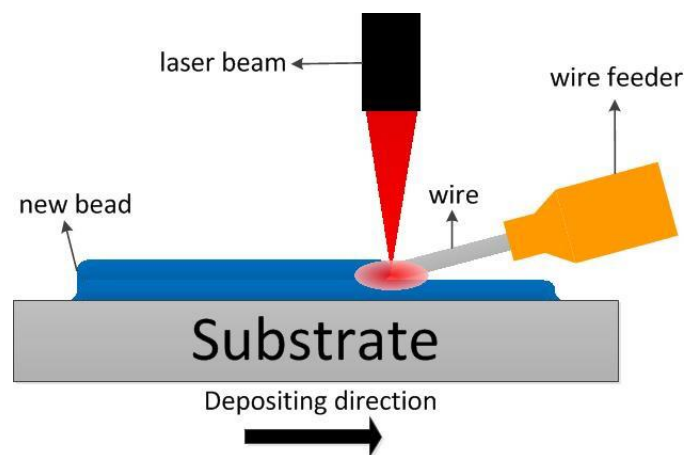


Figure 2.4 Laser metal deposition-wire (LMD-w), (Hryha, 2019)

## 2.4 Welding process

The welding process involves the material in the weld path which is heated, melted, and solidified within a specific time depending on the process conditions, which results in large temperature gradients and complex deformation paths (Xuan Liang L. C., 2018). The process of AM simulation is generally equated to the welding process simulation. The process of AM is a series of micro-welding in a controlled path flow. Thus, the theories of welding simulation are applicable for the AM processes (Nils Keller, 2014).

## 2.5 Strain

The Strain is defined as the relative change in shape of a cubic material and it can be expressed as a change in size or angle of the material cube. The relation between stress and strain is depicted in Figure 2.5. Plastic strain in which the distorted body does not return to its original size and shape even after the deforming force is removed. It can also be called as permanent strain. Elastic strain in which the distorted body returns to its original shape and size when the deforming force is removed. It can also be called a temporary strain.

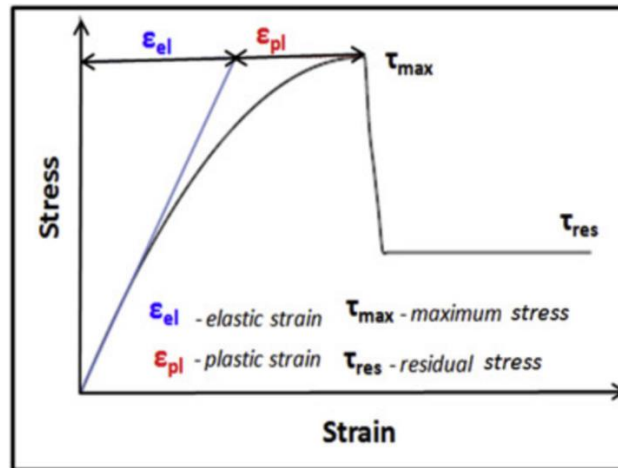


Figure 2.5 Relation between stress and strain to determine the elastic strain and plastic strain

## 2.6 Finite element analysis

### 2.6.1 Thermo-mechanical analysis:

TM analysis is one of the most used approach to predict residual stress and distortion for AM. In TM analysis, for an applied thermal load, the deformation and stresses are calculated that resides in the component. There are several commercial FEA software that can be used to capture these behaviors.

The TM analysis is divided into two cycles. First, the thermal cycle where the thermal effects are computed. The computed thermal effects are provided as input for the second cycle i.e., mechanical cycle in which the mechanical effects are calculated. Coupling the thermal and mechanical cycles is called a staggered approach. In this approach, the thermal cycle is solved iteratively until the solution converges. The material property is updated every time for each thermal cycle. The temperature field and the updated material-dependent temperature property is used as an input to the mechanical cycle. The mechanical cycle is also solved iteratively until the solution converges. The process flow of TM analysis is shown in Figure 2.6



Figure 2.6 Overview of flow in a TM analysis, (Mattsson, 2015)

### 2.6.2 Original Inherent strain theory:

Generally, the residual stress induced on a body after the welding process is the result of thermal strain, mechanical strain, shrinkage strain, creep strain, and phase transformation strain. These strains are caused by the heat source (M. G. Yuan, 1996).

Mathematically the total strain equals the elastic strain, plastic strain, thermal strain, phase transformation strain, and creep strain Eq.(1) (Iñaki Setien, 2019).

$$\varepsilon^{Total} = \varepsilon^{elastic} + \varepsilon^{plastic} + \varepsilon^{thermal} + \varepsilon^{phase\ change} + \varepsilon^{creep} \quad (1)$$

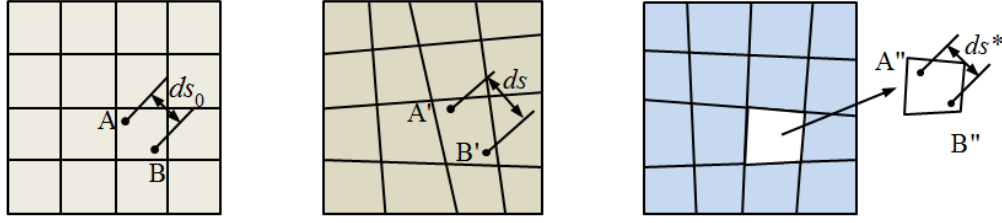


Figure 2.7 Different states for the definition of the inherent strain undeformed state (left), stressed state (middle), and stress relived-state (right) (Xuan Liang L. C., 2018)

According to (Xuan Liang L. C., 2018), let us consider two points in a material, A and B. The distance between the two points in the original (undeformed state) state is  $ds_0$ , and the stressed state is  $ds$ . After relieving the residual stress by removing the infinitesimal element containing two points. The distance between those points in the stress-relieved state is  $ds^*$ . Different states of the inherent strain are shown in Figure 2.7. The inherent strain is defined as the ratio of the change in the distance in the stress-relieved state and original state to the original state Eq.(2). The phase change and creep strain are neglected for simplification.

$$\varepsilon^{inherent} = \frac{(ds^* - ds_0)}{ds_0} \quad (2)$$

In the welding process, the material is cooled to the ambient temperature and hence, the thermal strain is removed.

$$\varepsilon^{inherent} = \frac{(ds - ds_0)}{ds_0} - \frac{(ds - ds^*)}{ds_0} \quad (3)$$

Under the assumption of infinitesimal deformation  $ds_0$  is approximately the same as  $ds$ .

$$\varepsilon^{inherent} = \frac{(ds - ds_0)}{ds_0} - \frac{(ds - ds^*)}{ds} \quad (4)$$

The first part of the right side is total mechanical strain and the second part is total elastic strain Eq.(4). The total elastic strain is removed because the elastic strain is directly proportional to the stress relieved, thus the elastic strain vanishes.

$$\varepsilon^{inherent} = \frac{(ds - ds_0)}{ds_0} \quad (5)$$

For the application of this theory into practice, the key assumption is that the elastic strain is not as important as plastic strain. Thus, the equation becomes total inherent strain is equal to the total mechanical strain or plastic strain Eq.(5).

### 2.6.3 Modified theory Inherent strain

For the AM process the elastic strain cannot removed as done in the traditional welding simulation. Since the process of AM is different from the traditional welding process. In the AM process every new layer added is constrained mechanically. Once there are multiple layers added, the previous layer changes to the steady-state. So, the elastic

strain in the AM will contribute to the distortion occurred in the part (Xuan Liang L. C., 2018). The traditional inherent strain theory is therefore not applicable to the AM process, because of the multi-layer effect in the AM process (Qian Chena, 2019).

AM material deposition is classified as initial deposition, intermediate state, and steady-state. The initial deposition is the first deposition of material on the substrate. The intermediate state is the state when the source of heat is just moved to the adjacent location for a deposition. Steady-state is the state in which the whole model is cooled to ambient temperature.

$$\varepsilon^{inherent} = \varepsilon_{intermediate\ state}^{plastic} + \varepsilon_{intermediate\ state}^{elastic} - \varepsilon_{steady\ state}^{elastic} \quad (6)$$

According to (Xuan Liang L. C., 2018), the inherent strain is defined as the difference between the mechanical strain at the intermediate state and the elastic strain at the steady-state Eq.(6). The intermediate state is a direct result of the solidification process. The generated mechanical strain is highly localized to that point. Also, these two states are associated with strain formation within a localized points due to the process of material melting and solidification (Qian Chena, 2019).

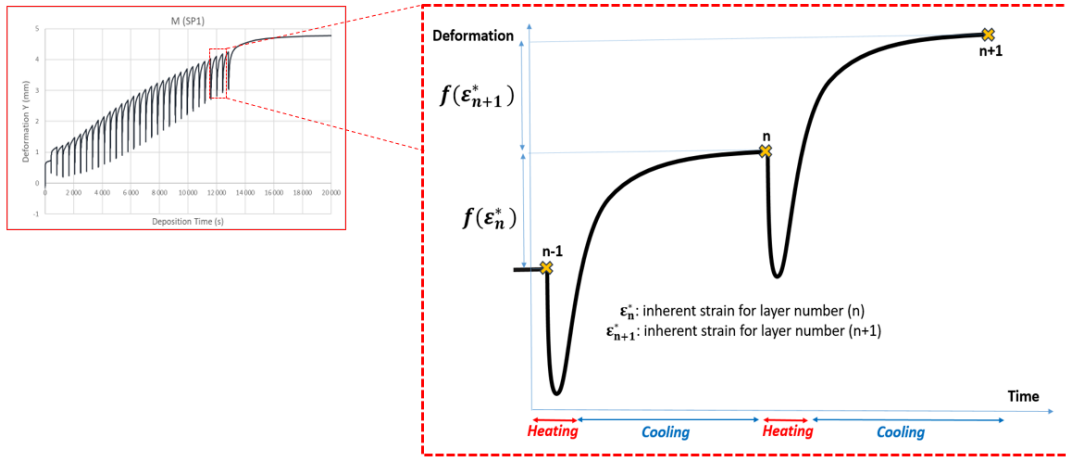


Figure 2.8 Inherent strain curve

In brief, the inherent strain theory is shown in Figure 2.8. The figure in the left corner illustrates the deformation occurred over the deposition time for (n) number of layers. Let us consider the deformation curve for one layer of deposition. An individual weld pass consists of a heating and a cooling cycle. Due to this thermal cycle, deformation occurs in the product. According to the modified inherent strain method, the deformation caused by the thermal cycle is replaced by  $(\varepsilon_n^*)$  inherent strain tensor for that layer which balances the constitutive stress that occurred.

## 2.7 Sub structuring

In the AM process all layers must be combined, the components normally consist of several thousands of layers. Simulation of individual layers requires a large range of calculations. Furthermore, it is time-consuming and may take several weeks (Nils Keller, 2014). the method of inherent strain is applied to a small block or representation of the real model. Because applying the method to a large-scale product increases the complexity and time. Also, it requires extensive computational power (Matteo Bugatti, 2018).

Sub structuring is a method where the global model is condensed into a simplified model with minimum features or a local model retaining all the features of the global model. The sub structuring approach is a process of splitting the meshed global model into a condensed local model. The mesh type remains the same for both the global and local model. In a welding simulation, the local model is treated as a non-linear model. The boundary condition and load cases applied for the local model is the same as the global model. Using this technique, the (Lundbäck, 2010) succeeded to reduce the computational cost. It is important to keep the part model long enough to include all non-linear phenomena involved in the Finite element method. In Figure 2.9 an example of the concept of sub structuring is illustrated.

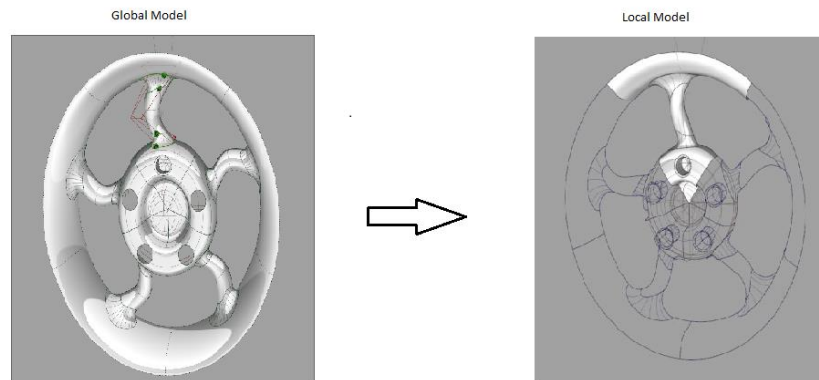


*Figure 2.9 Example of sub structuring*

## 2.8 Element birth and death technique

The element birth and death technique is used to reduce the time and predict the deformation of the mechanical problem of a part swiftly. In AM simulation the stress, temperature, and displacement at a certain point in a layer are affected by the number of previous layers deposited. The process of the layer-based element birth and death technique is shown in Figure 2.10.



*Figure 2.10 Element birth technique*

In this modelling, initially, all mesh elements are deactivated. The elements are activated in a layer-wise fashion upon the built direction. The inherent strain to be calibrated is applied in each activated layer (Nils Keller, 2014). Figure 2.11 illustrates the layer-by-layer method of assigning inherent strain. The inherent strain will be applied at the steady-state to each deposition layer. Since it is dominant at the steady-state of the laser scanning (Xuan Liang Q. C., 2019).

### Two-layer deposition modeling:

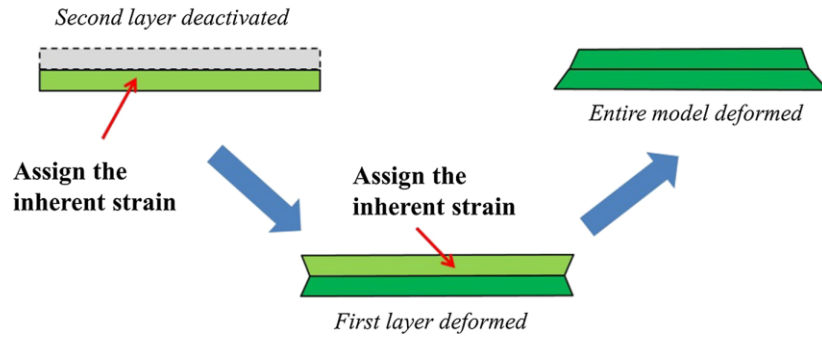


Figure 2.11 Two-layer example for illustration of the layer-by-layer method of assigning the inherent strain (Xuan Liang Q. C., 2019).

## 2.9 Calibration of inherent strain tensor

To calibrate the inherent strain tensor a simple regression optimization problem is formulated. The strain tensors are calibrated based on the target deformation contribution computed from the TM analysis  $d_{TM}$  and the deformation contribution computed from the static mechanical analysis  $d_M$ . Where,  $r_i$  - difference between  $d_{TM}$  and  $d_M$ ,  $i$  - counter,  $n$  - the number of sample points.

$$D = \min \sum_{i=1}^n r_i^2$$

### 3 Methodology

In this chapter, the methodology used in performing this thesis work is presented.

#### 3.1 Multi-scale approach

The multi-scale modeling approach is applied for the laser powder bed fusion process (Michael Gouge, 2019). In this master thesis, the approach is adapted for the inherent strain modeling method. The multi-scale modeling of AM processes is divided into two different scales of simulation, 1) small-scale model or mesoscale model, 2) Large-scale model, or part-scale model. Small scale model is a simple and scaled-down representation of the large-scale model. Fan case is the large-scale model. The Figure 3.1 depicts the sub structuring of fan case to different subscale models. In this thesis, the influence of the small-scale model geometry is studied in detail to validate the results between the simulations.

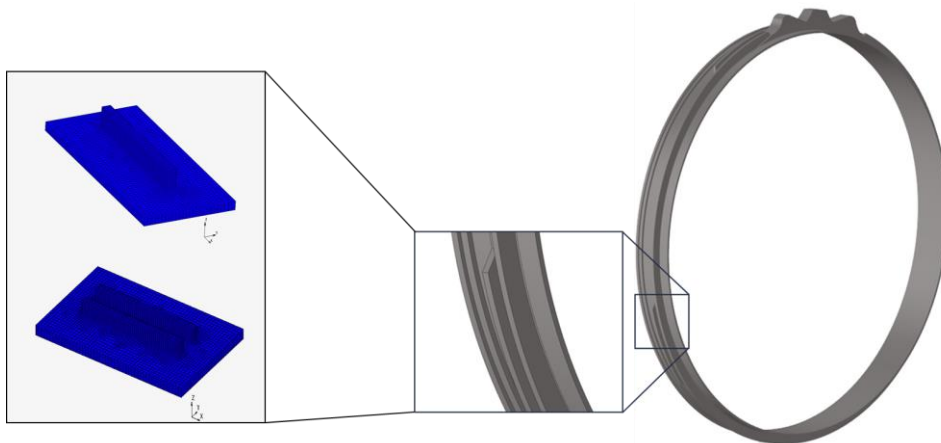


*Figure 3.1 Sub structuring of fan case (right) to subscale models (left)*

The multi-scale modeling described in Figure 3.2 consists of two stages of simulation. First the TM simulation for the small-scale model. Second, a mechanical simulation for the small-scale model, in this stage the calibration of inherent strain tensors is done with respect to the target deformation. The two stages of the simulation are done for all the small-scale models. To evaluate the best configuration of the small-scale model, a sensitivity study on inherent strain tensor is done on fan case (large scale model). Finally, the inherent strain tensor from the sensitivity analysis and inherent strain tensor from the inherent strain method is compared and analyzed. As mentioned earlier the inherent strain tensors are isotropic. In all the stages explained above the process parameters and material parameters are set constant throughout the process. A similar approach has been used successfully on a large-scale aerospace part (Ploshikhin, 2010).

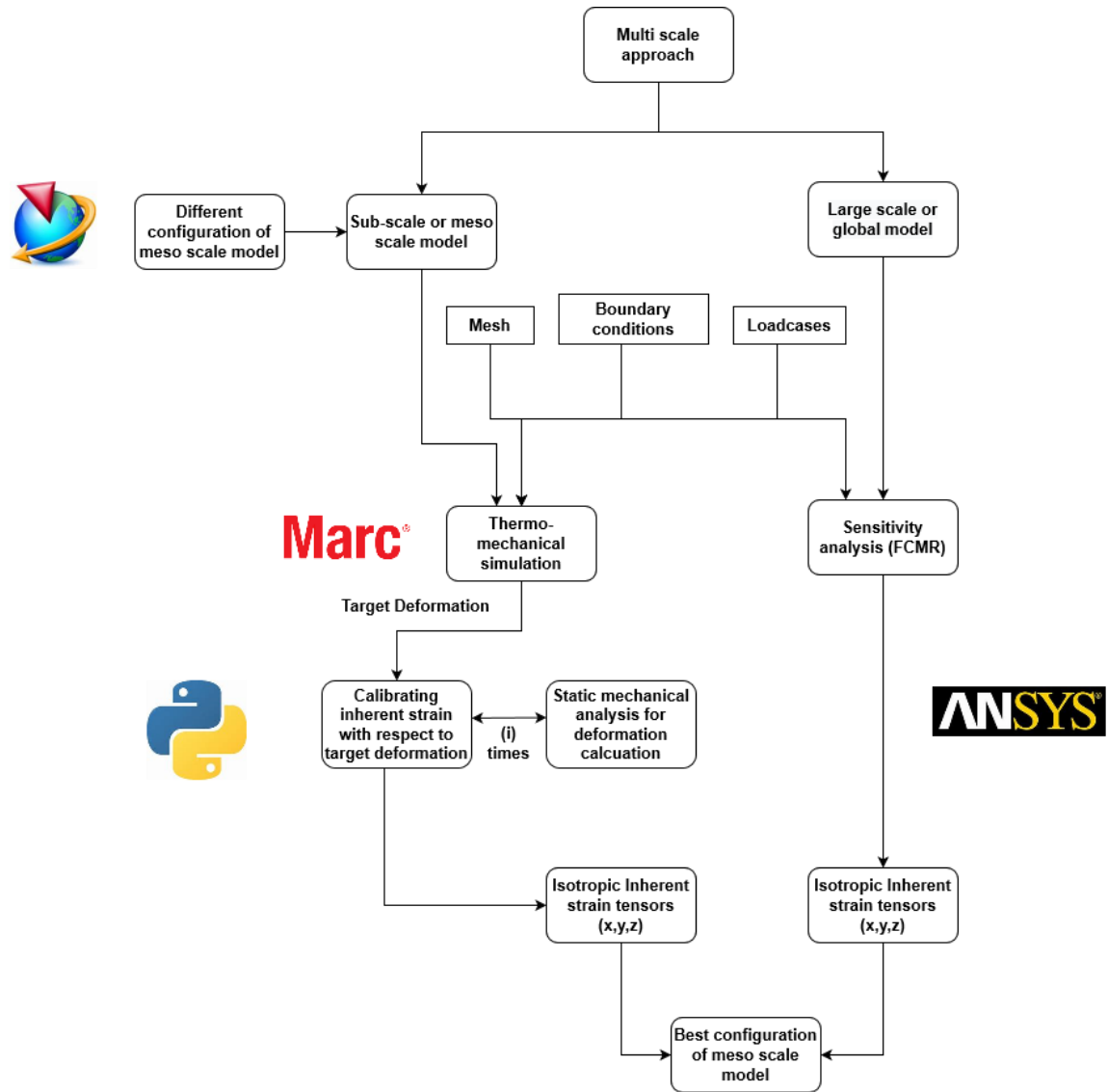


Figure 3.2 Flow chart of Multi-scale approach

## 4 Workflow

In this chapter, the CAD models of the subscale model are explained. Also, the modeling procedure such as load case, boundary conditions, and the meshing strategy is presented.

### 4.1 CAD Models

In this thesis work, seven different geometric small-scale models were prepared and analysed to study the influence of the geometry of the small-scale models. These CAD models were classified into three configurations i.e., the layer configuration, geometric configuration, and weld path configuration. In the layer configuration, the layers of the bead deposition were changed. In the second configuration geometry of the small-scale models was modified from a simple model to a more featured model resembling the large-scale model. In weld path configuration the weld path was modified as subsequent deposition and parallel deposition.

#### 4.1.1 Layer configuration

The thesis primarily aims to reduce the computational time taken by TM analysis. The number of bead layer deposition significantly affects the computational time in the TM analysis. Thus, at the beginning of this thesis, different layer combination was modeled and evaluated. In the layer configuration, the three models were modeled with similar geometry except for the bead deposition layer height. There were three deposition layers namely 17 layers, 29 layers, and 10 layers.

##### M1:

The model M1 has 17 layers of the bead and five layers of the substrate part. The model consists of 15183 nodes and 12050 elements of Hexa-8 elements.

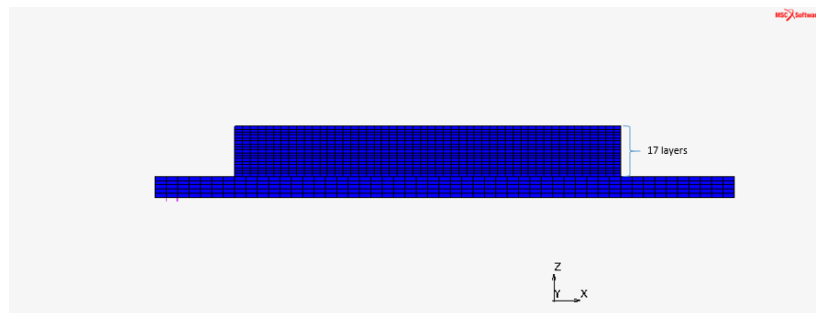


*Figure 4.1 M1- 17 layer of bead*

##### M2:

The model M2 has 29 layers of the bead and five layers of the substrate. The model consists of 18411 nodes and 14595 elements of Hexa-8 elements.

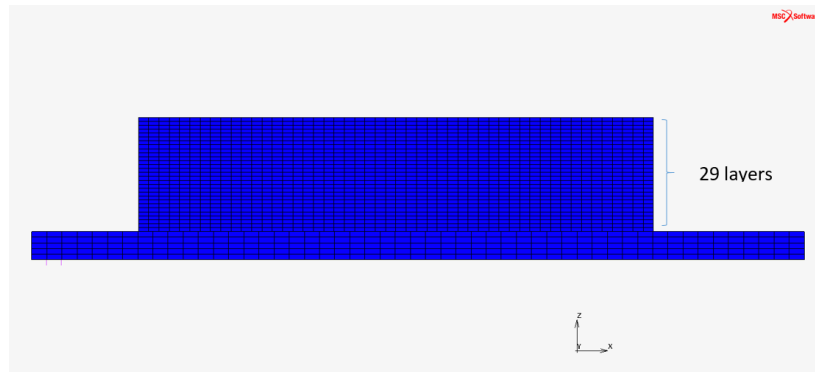


Figure 4.2 M2- 29 layers of bead

**M3:**

The model M3 has 10 layers of the bead and five layers of the substrate. The model consists of 13566 nodes and 8795 elements of Hexa-8 elements.

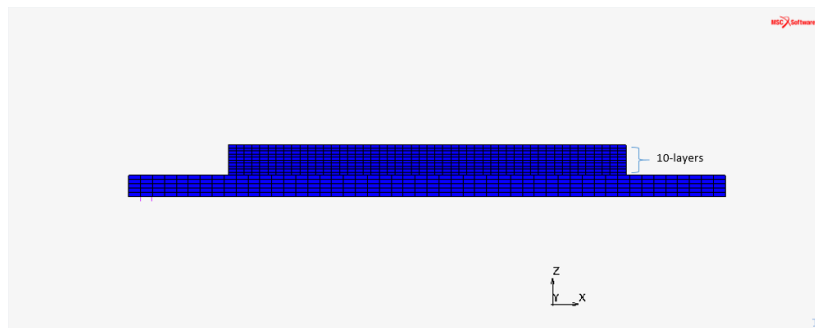


Figure 4.3 M3- 10 layers of bead

**4.1.2 Geometric configuration**

In geometric configuration, the geometric properties are modified such as the width and including two bead wall deposition.

**M4:**

The model M4 has 17 layers of the bead and five layers of the substrate. The model consists of 15183 nodes and 12050 elements of Hexa-8 elements. The bead deposition is symmetric with respect to the width of the substrate whereas it is asymmetric with respect to the length of the substrate.

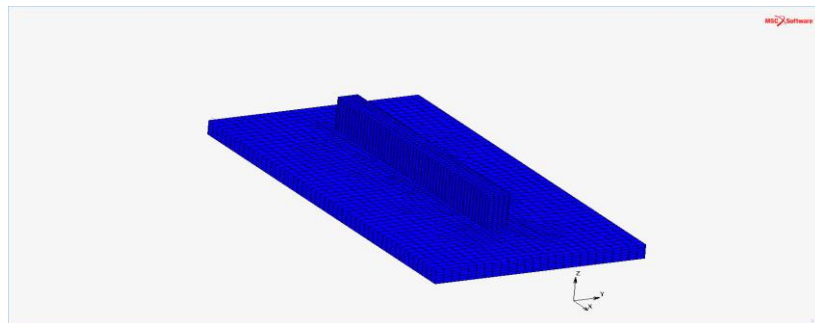


Figure 4.4 M4- 16 layers of bead

**M5:**

The model M5 has two 10 layers of bead deposition and five layers of the substrate. The model consists of 13566 nodes and 8795 elements of Hexa-8 elements.

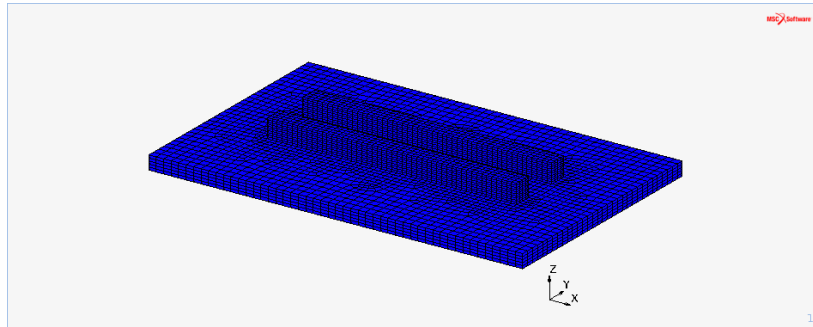


Figure 4.5 M5- Two bead deposition

### 4.1.3 Weld path configuration

In weld path configuration the weld path or the deposition path was modified to improve the model further and simulated the model more realistically. The weld path configuration is considered for the models that have two bead parts for deposition. Two different weld path configurations were modeled parallel weld path and subsequent weld path. In parallel weld path the deposition layers on either walls are built parallelly. Whereas in the subsequent weld path, all the deposition layer in one wall is built completely and then the second wall is initiated.

#### M6:

The model M6 has two 10 layers of bead deposition and five layers of substrate. The model consists of 20004 nodes and 16005 elements of Hexa-8 elements. For this model, the weld path is defined as parallel weld path. The bead deposition has 10 layers each. The geometric properties of model M5 and M6 are similar.

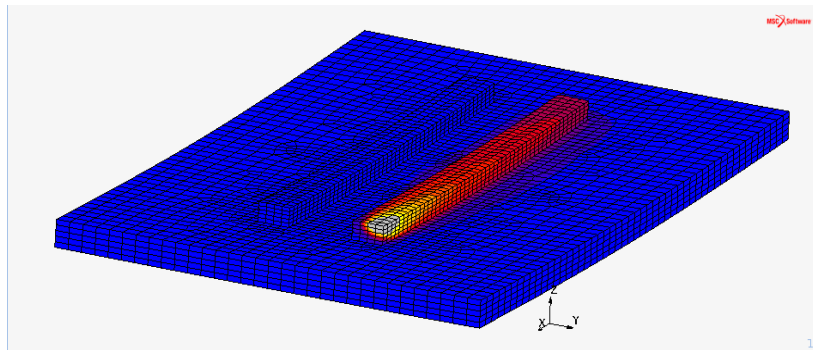


Figure 4.6 M6- Parallel weld path configuration

#### M7:

The model M7 has two 29 layers of bead deposition and 5 layers of substrate. The model consists of 29694 nodes and 23605 elements of Hexa-8 elements. For this model, the weld path is defined as subsequent weld path. The bead deposition has 29 layers for each wall.

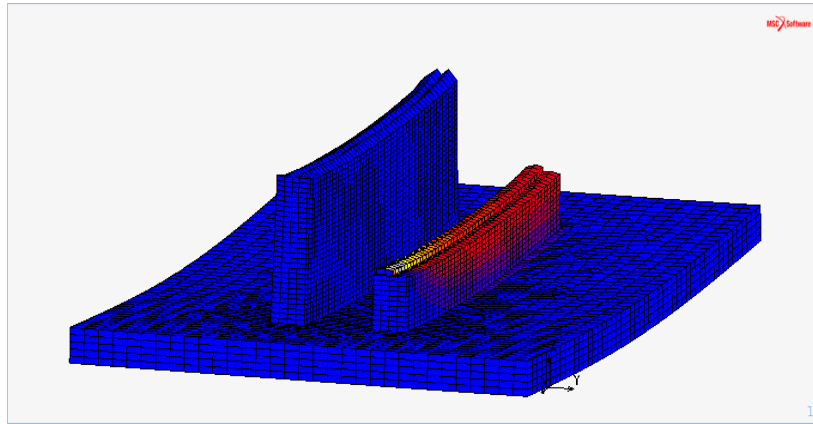


Figure 4.7 M7- Subsequent weld path configuration

## 4.2 Material

Ti-6Al-4V is the material used throughout the simulation for both the fan case and the small-scale models. Ti-6Al-4V also called Ti64, possesses a high performance with respect to strength, heat, fatigue resistance, toughness, and corrosion resistance. Different compositions of the elements in Ti64 possess different properties and usage. The composition details of Ti64 is mentioned in Table 4.1 (CESEduPack, 2019).

Table 4.1 Ti64 material composition

Element	Composition (%)
Al (aluminium)	5.5 – 6.75 %
C (carbon)	0 – 0.1 %
Fe (iron)	0 – 0.4 %
H (hydrogen)	0 – 0.0125 %
N (nitrogen)	0 – 0.05 %
O (oxygen)	0 – 0.2 %
Ti (titanium)	88 - 91 %
V (vanadium)	0 – 0.4 %

## 4.3 Weld path

Different weld path strategies that can be considered while producing a part using the AM process. It appears that the different kind of strategies results in different stress state and distortion (Sonja Jonsson, 2018). Whereas in this thesis the horizontal weld path strategy is used to keep the model and simulation as simple as possible. Figure 4.9 illustrates the weld path and its orientation path. The red cross in Figure 4.9 is the defined weld path of the first pass of each layer and the green dot is the orientation path of the respective weld pass. In an n-layer of deposition, two weld passes occur for each layer deposition.

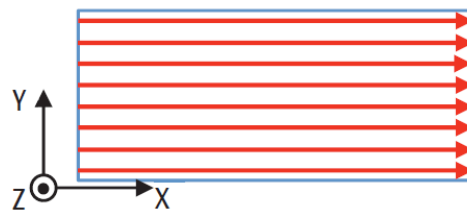


Figure 4.8 Horizontal direction scanning strategy (Sonja Jonsson, 2018).

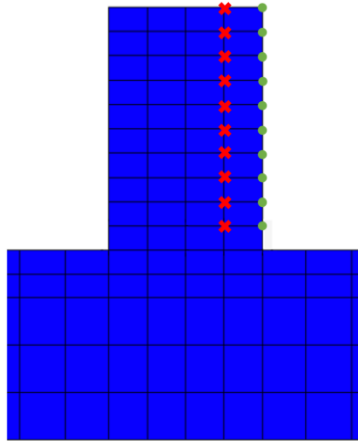


Figure 4.9 Visualizing of weld path, red crosses marks the weld paths and green dots marks the orientation paths (Forslund, 2018)

## 4.4 Meshing

All the models in this thesis are meshed in a similar approach. The models have meshed as two parts AM build part and substrate. The AM build part is considered as a heat-affected zone (HAZ) to ensure accuracy in results the HAZ part is meshed finer when compared to the substrate. HAZ is divided into n-number of layers, and each layer in the HAZ is divided equally into one element vertically and four elements horizontally. A fine mesh is used in the HAZ and a coarse mesh is used for the substrate part to reduce the complexity of the model.

In mechanical analysis element type “Solid185” is used for 3-D modeling of solid structures in ANSYS. It is defined by eight nodes having three degrees of freedom at each node. For a TM simulation element type “7” is an eight-node, isoperimetric, arbitrary hexahedral element used in MSC Marc.

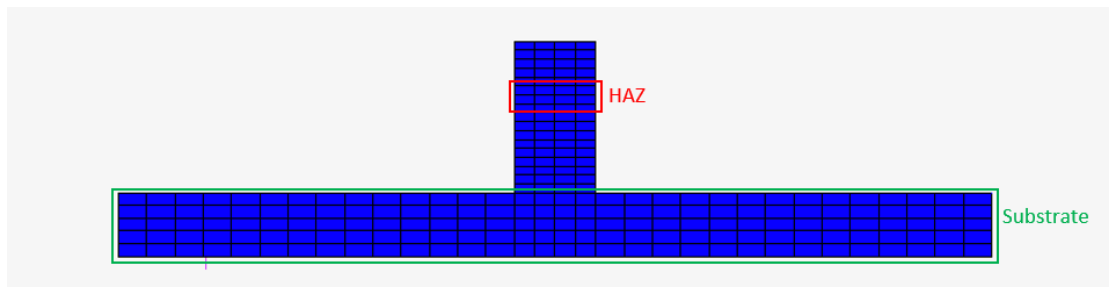


Figure 4.10 Mesh

## 4.5 Boundary Condition

In both the simulation the initial condition is set as the temperature on all the nodes in the model to 293 K (20°C). The model consists of two Boundary Conditions (BC) mechanical and thermal boundary conditions.

The mechanical boundary condition is applied to the bottom surface of the substrate. Throughout the simulation, the bottom surface is fixed until the last load case. Also, there is a BC applied to release all the other mechanical BC after the last load case, to obtain the final deformation. A Schematic view of mechanical BC is shown in Figure 4.11.

Thermal volume flux, convection, and radiation are applied as thermal BC in this model. One thermal volume flux for each weld pass is created and applied to all the elements in the HAZ and is applied to all the elements in the substrate adjacent to it. Radiation and convection BC is applied to all the faces involved in the material melting and cooling phase of the process in a layer-wise manner. The heat transfer is modeled by using thermal face film with a defined film coefficient describing the amount of heat passing through that area. The conduction boundary condition is applied to all the elements that would experience the heat source. The transfer of heat is modeled by using thermal volume flux.

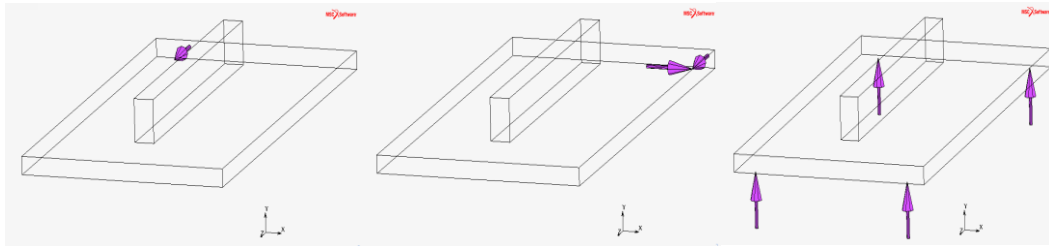


Figure 4.11 Mechanical boundary condition

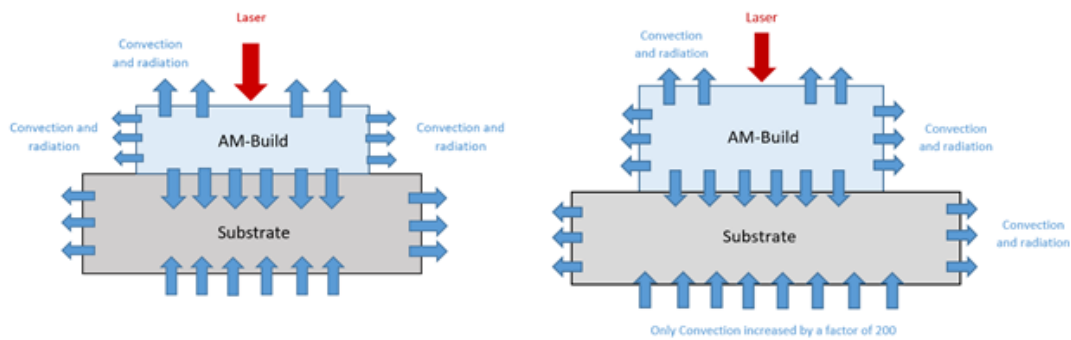


Figure 4.12 Schematic view of the thermal boundary condition BC1(left) and BC2(right)

In this thesis work, two thermal boundary conditions were applied. For the initial analysis of the subscale models, BC1 was used. In the later stage of the thesis work, BC2 was used. In BC2 a more realistic thermal boundary conditions were applied by increasing the film coefficient of convection by a factor of 200. Also, the radiation passing underneath is removed as shown in Figure 4.12. The BC2 was applied to represent the exact thermal conditions of the large-scale model.

## 4.6 Load cases

In TM the load case is defined for each pass of the layer deposition process. There are four load cases for each deposition. The sequence of the load is shown in Figure 4.13. A welding load case is applied initially, followed by a cooling load case. The weld cycle time and cooling time data are taken from the real-time process. Once the last load case

is applied, the fixed BCs are released and the modeled is cooled to the ambient temperature.



Figure 4.13 Load case for TM simulation

For mechanical analysis, the element birth techniques is used for element activation and deactivation, it is explained in Section 2.8. Figure 4.14 illustrates the load case for a mechanical analysis. All the layers are deactivated initially and activate the layer where the inherent strain tensors are being applied. This process is repeated up to n number of layers.

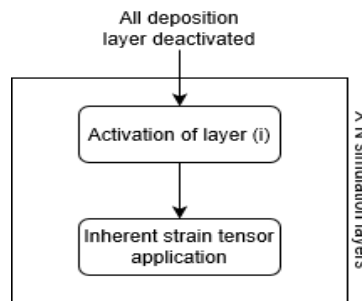


Figure 4.14 Load case for mechanical analysis

## 4.7 Calibration

The calibration problem is explained in Section 2.9. In this thesis work, the inherent strain tensors are calibrated for four layers, irrespective of the number of layers involved in the bead deposition. The four layers are 1<sup>st</sup> layer, 2<sup>nd</sup> layer, intermediate layers, and the final layer.

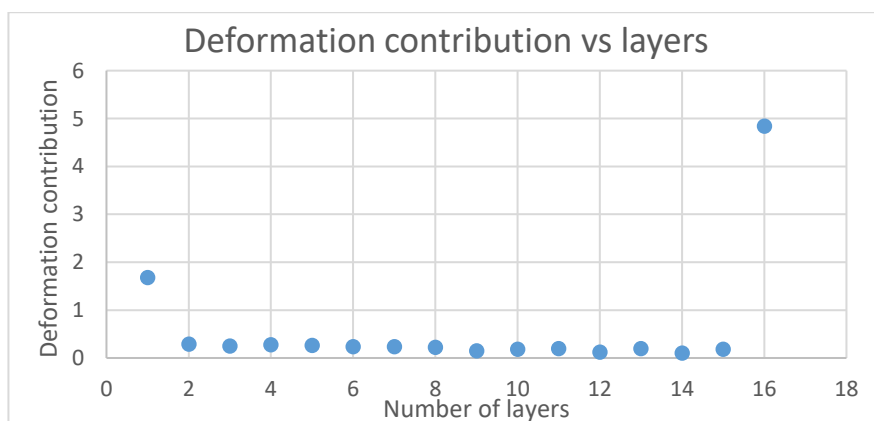


Figure 4.15 Deformation contribution vs number of layers

In Figure 4.15 the deformation contribution per layer is shown. From the graph, it authorizes the selection of the four layers for the calibration process. There is a transient change in the deformation contribution between the 1<sup>st</sup> and 2<sup>nd</sup> layers. Also, the process parameters slightly differ between the 1<sup>st</sup> layer and the remaining layers in the bead deposition. From the graph, we can verify that the change in deformation contribution

in the intermediate layers is marginal. Thus, in the calibration process the average deformation contribution is computed for the intermediate layers alone, and finally, the final layer is calibrated because the bead deposition is completed, and the body is cooled to the ambient temperature. The inherent strain tensor used for the calibration process is mentioned in Table 4.2.

Table 4.2 Calibrated inherent strain tensor

Layers	Inherent strain tensors range	Step size
All layer	0.001-0.01	0.0005

## 4.8 Thermo-mechanical simulation

The TM simulation was performed in MSC Marc. TM simulation was performed to all the subscale models presented in Section 4.1. The load cases, boundary condition, mesh, weld path, and material is explained in detailed Section 4.2-4.5, Figure 4.16.

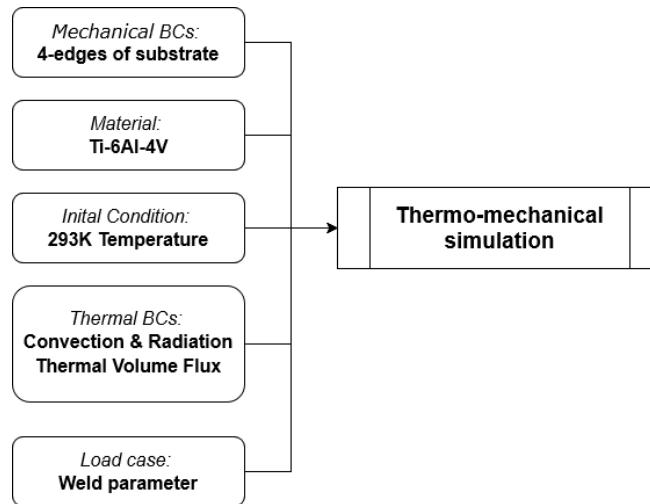


Figure 4.16 TM simulation

The primary purpose of the TM simulation is to extract the target deformation for the subjected simulation setup. The target deformation obtained from the TM simulation is used in the inherent strain method for the calibration of inherent strain tensors. The target deformation is extracted from three specific nodes Sp1, Sp2, and Sp3. The deformation at these nodes was maximum. The nodes are presented in Figure 4.17.

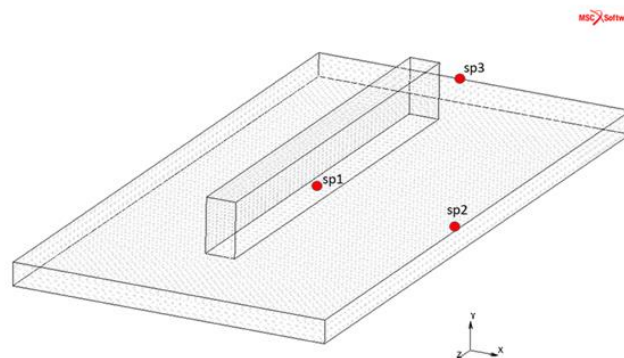


Figure 4.17 Nodes Sp1, Sp2, and Sp3 for extraction of target deformation

## 4.9 Inherent strain simulation

The inherent strain simulation was performed in ANSYS APDL and the calibration was done in python. The target deformation is obtained from the TM simulation. The deformation contribution is computed w.r.t to the deposition time. The mesh and mechanical BC are similar to the TM simulation. In the inherent strain method thermal BC is not applied. The mesh, load case, BC's are explained in Section 4.2-4.6. Static mechanical analysis is performed on all the subscale models by applying the inherent strain tensors as load case. The simulation setup is shown in Figure 4.18. The deformation contribution computed from the static mechanical analysis is compared with the deformation contribution computed from the TM simulation, a sum of square error is calculated and the best inherent strain tensor is identified.

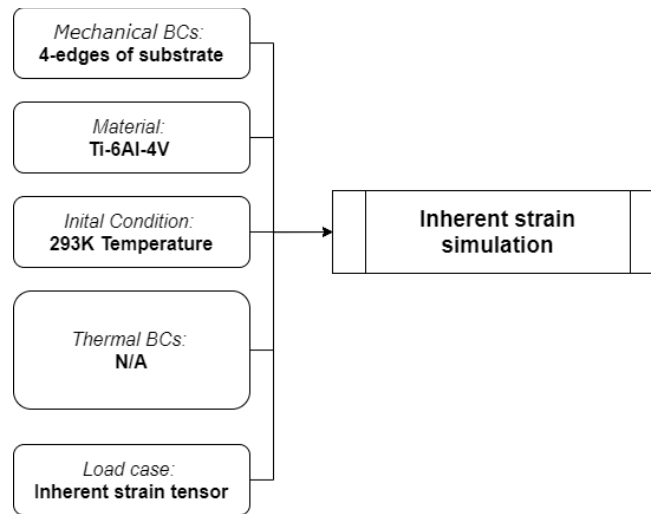


Figure 4.18 Inherent strain simulation setup

## 4.10 Sensitivity Analysis

A sensitivity analysis was performed on fan case to identify the best fit inherent strain tensor w.r.t to radial deformation. In this study, the inherent strain used for the calibration process was inserted in an iterative manner for each layer of deposition. The sensitivity analysis was done through the inherent strain method where the inherent strain tensors are inserted to each layer of bead deposition. The element birth technique explained in Section 2.8 is used for the element activation, deactivation, and application of inherent strain tensors. As used in the inherent strain method three isotropic inherent strain tensors are inserted into the model. The inherent strain tensors used in the study are mentioned in the Table 4.3.

Table 4.3 Inherent strain tensor used in sensitivity analysis

Layers	Inherent strain tensors range	Step size
1 <sup>st</sup> layer	0.006-0.01	0.001
Interim layer	0.001-0.01	0.001
Last layer	0.005-0.01	0.001

## 5 Results and Discussions

In this chapter, the results and findings from the simulation done in this thesis are presented. The results in this section are sub-divided into deformation results, calibration results, and sensitivity analysis.

### 5.1 Deformation Results

In this section, the deformation results for all the models are presented and described. The graphs illustrated in this section represent the deformation (mm) in the x-axis and the deposition time (seconds) in the y-axis.

#### 5.1.1 Layer Configuration

The deformation results for different layer configuration is shown in Figure 5.1. The graph illustrates the deformation over the deposition time. From the graph, the deformation follows a linear trend irrespective of the number of layer deposition. The trend that follows for the first ten layers in the M1 and M2 model is similar to the M3 model. Since the deformation contributed over the deposition time tends to follow a similar trend irrespective of the number of layers for deposition. It is better to use 10 layers for the bead deposition to reduce the computational time.

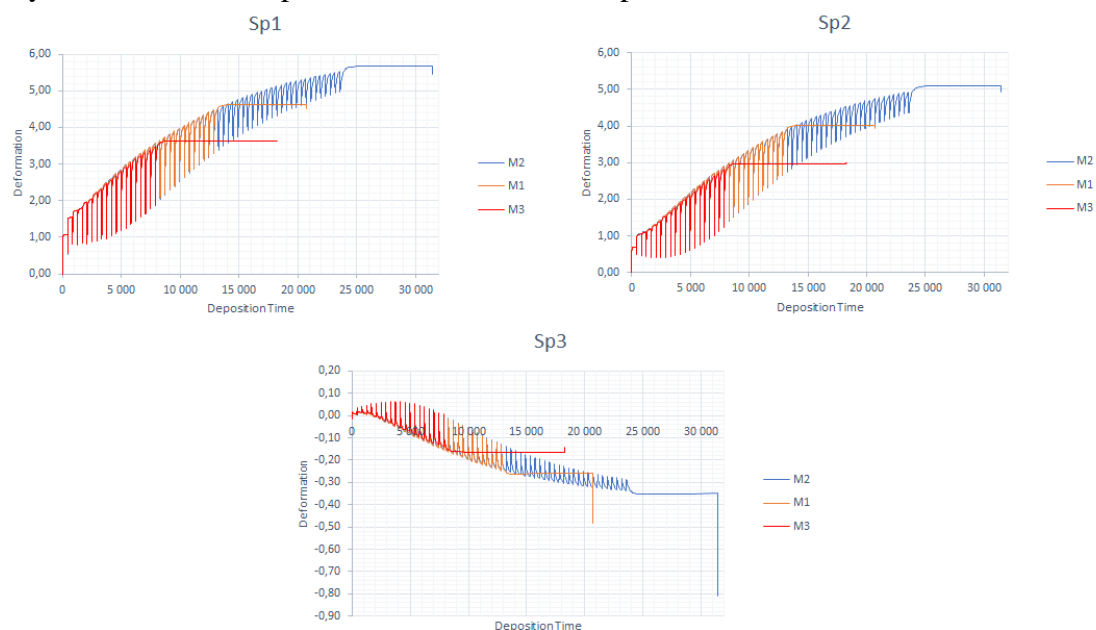


Figure 5.1 Deformation results for layer configuration M1, M2, and M3

#### 5.1.2 Geometric Configuration

The deformation results of the model M1 and M4 are illustrated in Figure 5.2. The result states that the asymmetry of the bead deposition in model M4 makes the model less stiff when compared to the model M1.

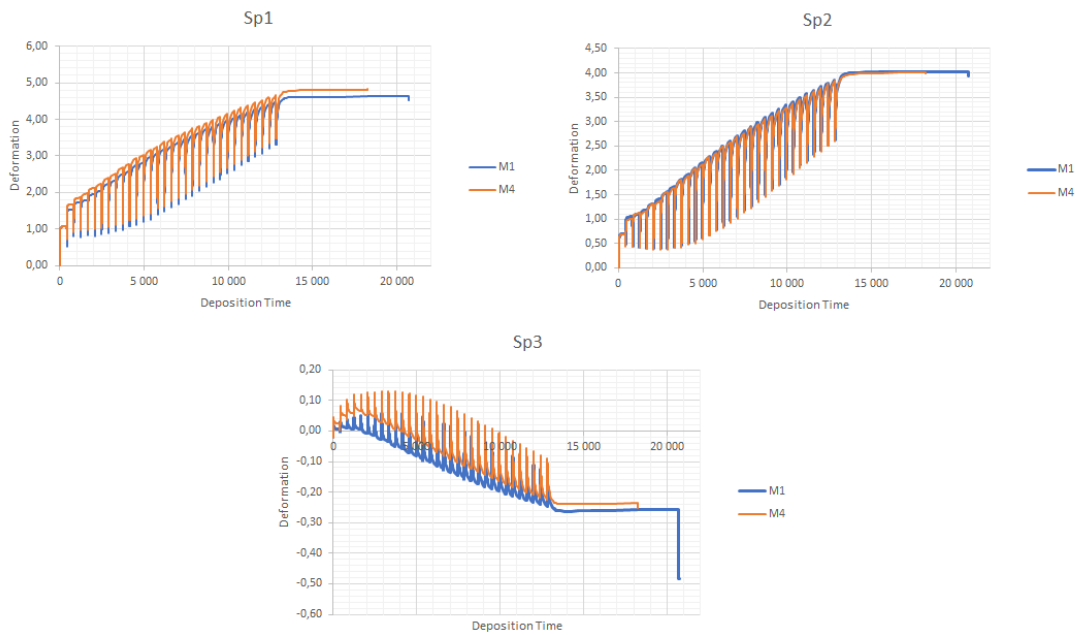


Figure 5.2 Deformation results for geometric configuration M1 and M4

### 5.1.3 Weld path configuration

The deformation results of model M5 and M6 is illustrated in Figure 5.3. The result states that the model with parallel weld path configuration M5 predicts higher deformation when compared with the model with subsequent weld path configuration M6.

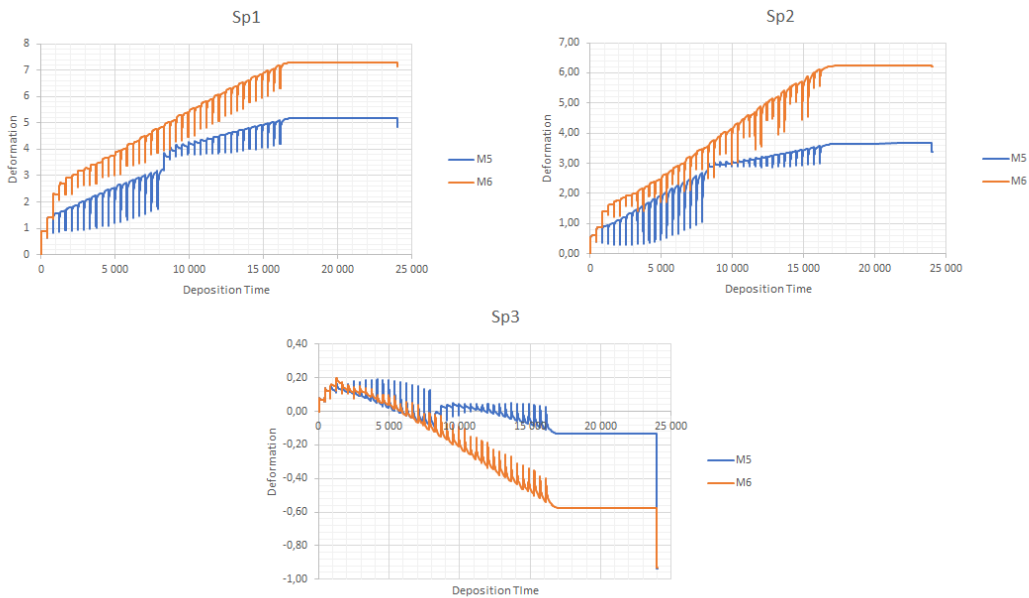


Figure 5.3 Deformation results for weld path configuration M5 and M6

## 5.2 Calibration Results

The inherent strain tensors are calibrated as described in Section 2.9 and 4.7. The graphs presented in this section represent the error in the deformation results between the inherent strain method and TM method in the x-axis and the inherent strain tensors in the y-axis.

## 5.2.1 Layer configuration

The models M1, M2, and M3 were simulated using the inherent method and the inherent strain tensors were calibrated accordingly. From Figure 5.4 it can be seen that the inherent strain tensor for the first, second, and interim layers are similar irrespective of the number of layers for deposition. The last layer alone shows a difference in the calibration results.

Table 5.1 Calibrated inherent strain tensors for M1, M2, and M3

Layers	M1 (x/y/z)	M2 (x/y/z)	M3 (x/y/z)
1st layer	0.0075	0.0075	0.0075
2nd layer	0.0025	0.003	0.0025
sInterim layer	0.003	0.003	0.003
Last layer	0.0065	0.0085	0.004

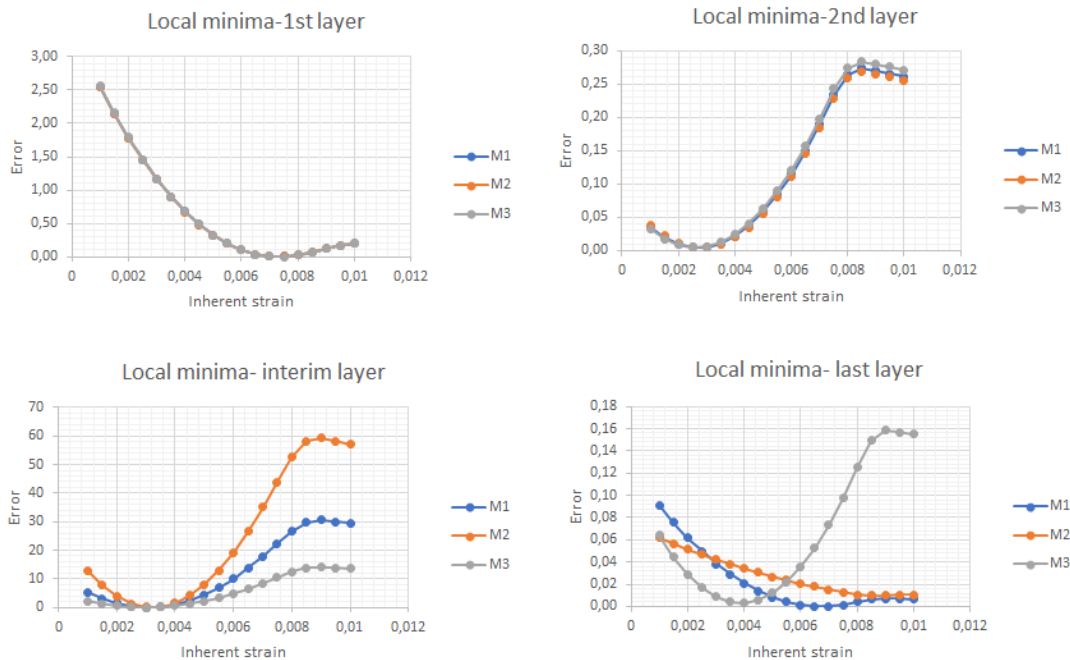


Figure 5.4 Calibration results for layer configuration M1, M2 and M3

## 5.2.2 Geometric configuration

The calibration results for the geometric configuration are shown in the Figure 5.5 and Table 5.2. In Figure 5.5 the results show that changing the geometric properties and stiffness of the models does not possess a difference in the inherent strain tensor calibration. The inherent strain tensors for the first, interim, and last layer are similar, and we can see a minimal difference in the error in the second layer. In Table 5.3 the calibrated results of model M5 and M7 are compared. It can be observed the inherent strain tensor for the first, second, and interim layers are similar. The inherent strain tensor for the last layer alone is approximately double between M5 and M7. These results reconfirm that the layer deposition does not influence the calibration of first, second, and interim layers, it only affects the last layer calibration.

Table 5.2 Calibrated inherent strain tensors for M1 and M4

Layers	M1 (x/y/z)	M4 (x/y/z)
1st layer	0.0075	0.008
2nd layer	0.0025	0.003
Interim layer	0.003	0.003
Last layer	0.0065	0.0065

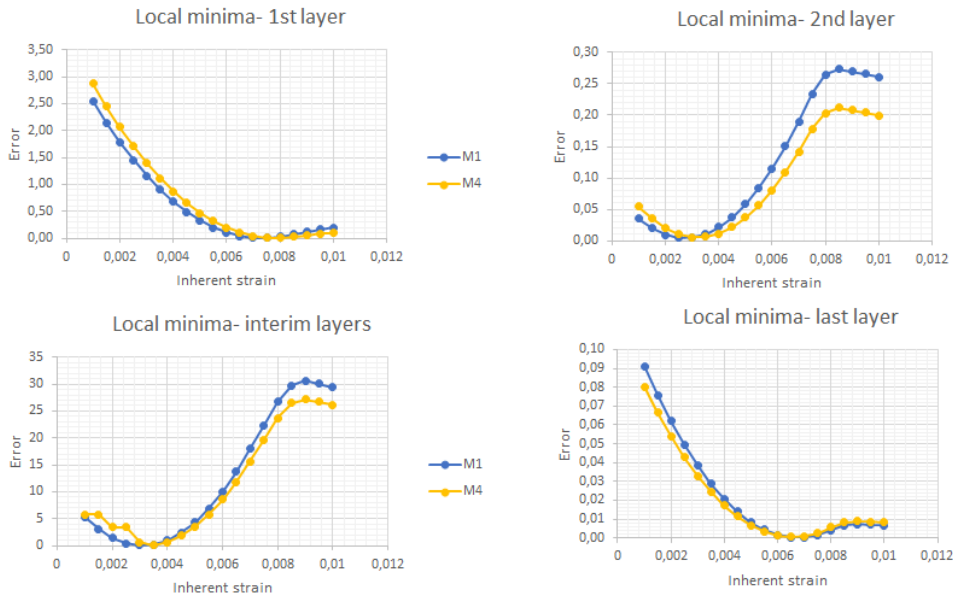


Figure 5.5 Calibration results for geometric configuration M1 and M4

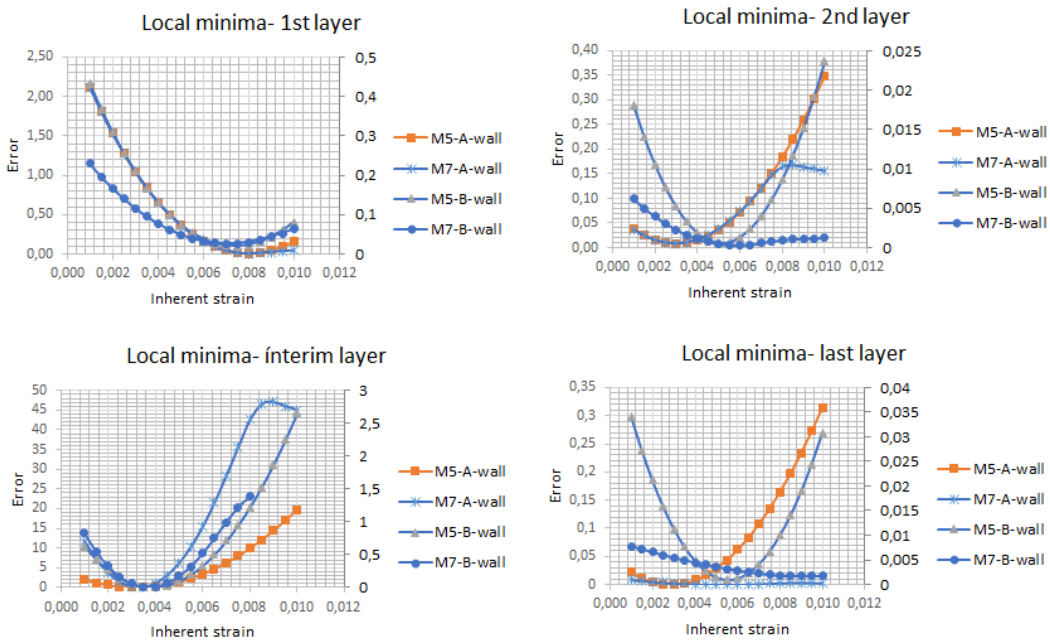


Figure 5.6 Calibration results for geometric configuration M5 and M7

Table 5.3 Calibrated inherent strain tensors for M5 and M7

Layers	M5 (x/y/z)		M7 (x/y/z)	
	A-wall	B-wall	A-wall	B-wall
1st layer	0.008	0.0075	0.008	0.007
2nd layer	0.003	0.005	0.003	0.005
Interim layer	0.003	0.004	0.003	0.004
Last layer	0.003	0.0055	0.0055	0.0085

### 5.2.3 Weld path configuration

Model M5 and M6 which is modeled with different weld path configurations are simulated using the inherent method and the calibrated inherent strain tensors are presented below. The results show that there is an increase in the inherent strain tensor in the interim and last layer. The first and second layer inherent strain tensor is comparatively equal.

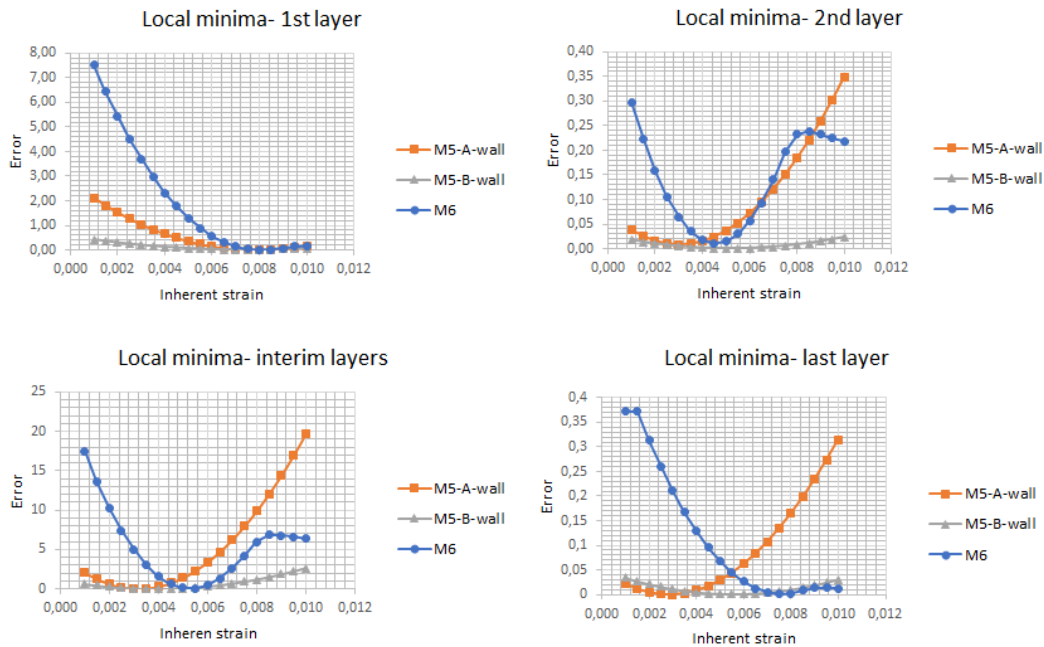


Figure 5.7 Calibration results for geometric configuration M5 and M6

Table 5.4 Calibrated inherent strain tensors for M5 and M6

Layers	M5 (x/y/z)		M6 (x/y/z)
	A-wall	B-wall	
1st layer	0.008	0.0075	0.008
2nd layer	0.003	0.005	0.0045
Interim layer	0.003	0.004	0.005
Last layer	0.003	0.0055	0.007

### 5.3 Sensitivity analysis results

The sensitivity analysis concludes that the radial deformation of the fan case is most sensitive to the interim layers due to added up deformation. The first and last layer seems to indicate a low sensitivity on the radial deformation. The sensitivity analysis results are shown in Table 5.5.

Based on the sensitivity analysis results for the different inherent strain tensors an error plot was plotted with respect to the inherent strain tensors. From the graph shown in Figure 5.8, for the first layer, there is a steep decrease in the error and at 0.01 the error seems to be minimum when compared to other strain tensors. In the intermediate layers, there seems to be an occurrence of convergence from 0.007 to 0.01 and the difference in error between 0.007 to 0.01 is approximately 5%. Thus, the best fit parameter for the interim layer is set as 0.007. For the last layer, 0.008 is the best fit parameter since the error at 0.008 is at the minimum.

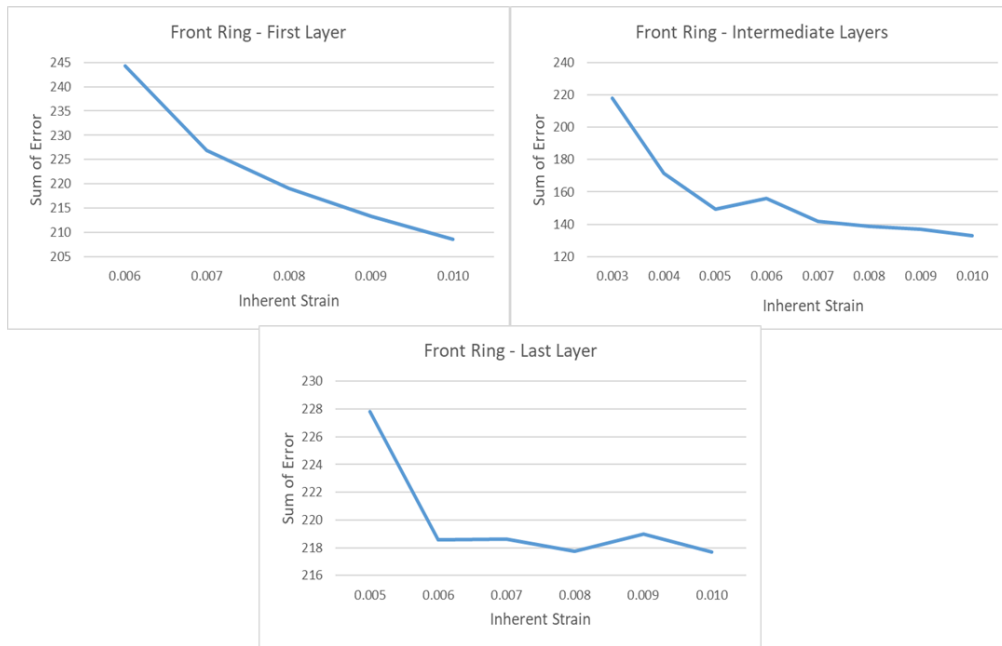


Figure 5.8 Sensitivity analysis error vs inherent strain tensor

Table 5.5 Best fit inherent strain tensor from sensitivity analysis

Layers	Inherent strain tensors
First layer	0.01
Interim layer	0.007
Last layer	0.008

## 5.4 New Thermal Boundary condition (BC2)

From the sensitivity analysis and initial analysis of the models. None of the subscale models, inherent strain tensor possesses a similar inherent strain tensor as found from the sensitivity study. Thus, an investigation on the thermal boundary condition was done as explained in Section 4.5. The BC2 was applied to the model M1.

### 5.4.1 Deformation Results

The new thermal boundary condition (BC2) was applied to the model M1. The deformation results shown in Figure 5.9 states that the deformation prediction in the BC2 is much higher when compared to BC1. This indicates that including a more realistic BC improves the accuracy of the prediction of deformation.

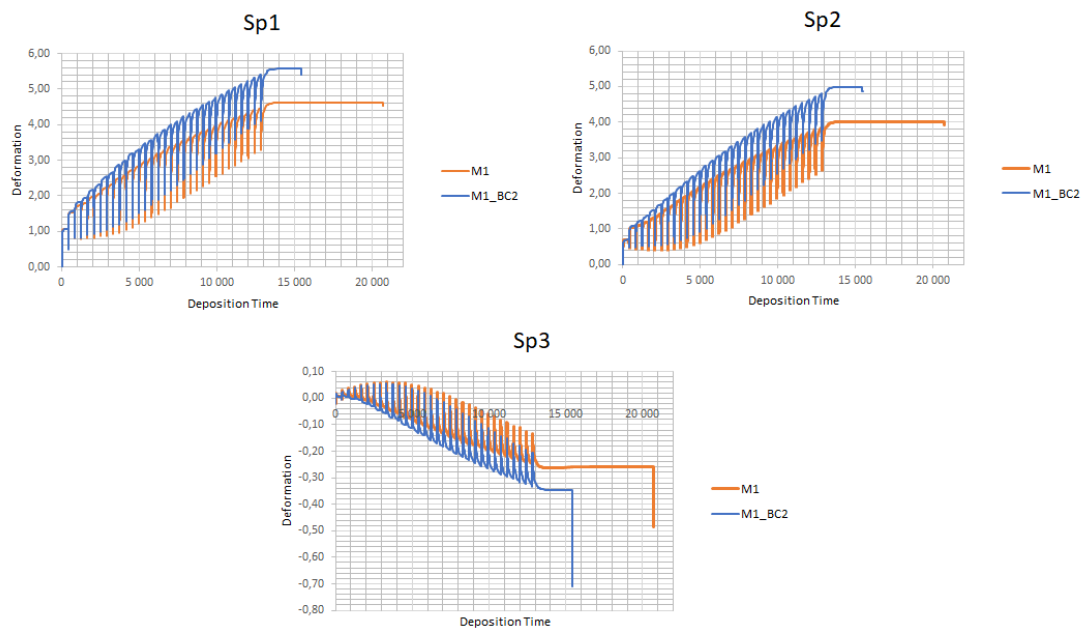


Figure 5.9 Deformation results for M1 with thermal boundary condition BC2

## 5.4.2 Calibration Results

The calibrated results for model M1 is presented in Figure 5.10 and Table 5.6. It seems that there is an increase in the inherent strain tensor in the second layer, interim layer, and last layer. Modeling a more realistic boundary condition improves the calibration results.

Table 5.6 Calibrated inherent strain tensors for M1 and M1\_BC2

Layers	M1 (x/y/z)	M1_BC2 (x/y/z)
<b>1st layer</b>	0.0075	0.0075
<b>2nd layer</b>	0.0025	0.0045
<b>Interim layer</b>	0.003	0.004
<b>Last layer</b>	0.0065	0.0075

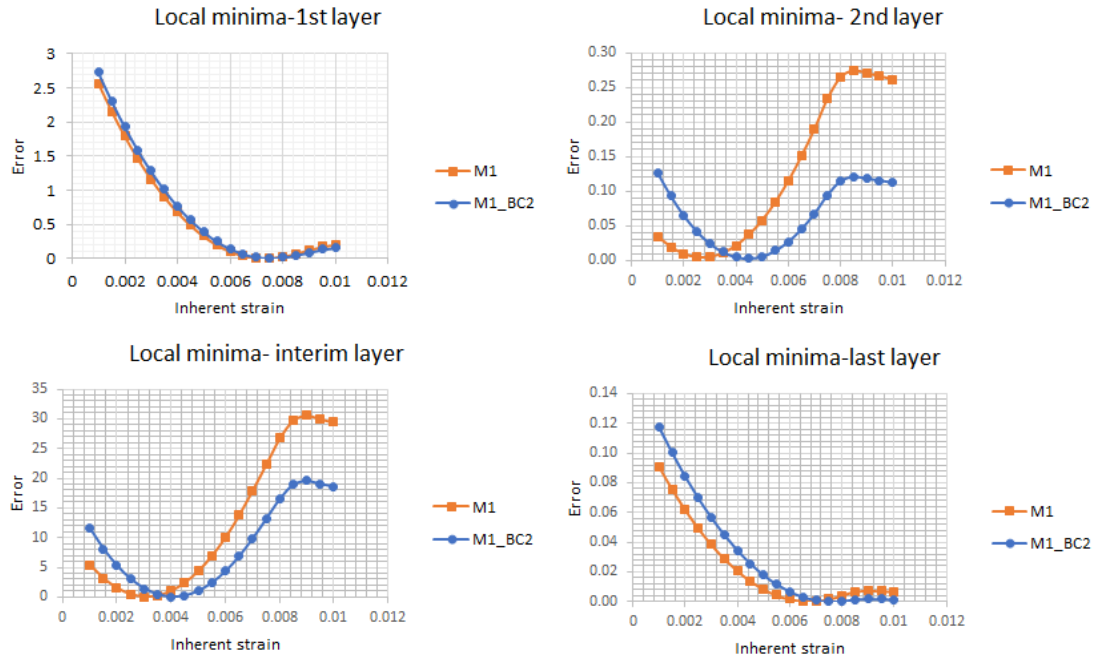


Figure 5.10 Calibration results for geometric configuration M1 and M1\_BC2

## 5.5 Time Evaluation

A time evaluation study was carried out in this thesis. The TM simulation time taken for each subscale model is presented in Table 5.7. From the computational time adding more features to the subscale model to represent the large-scale model will increase the computational time. Also, increasing the deposition layer will increase the computational time. From the layer configuration results using minimum layers will reflect the same result with minimum computational time.

Table 5.7 Time evaluation for the subscale model

Models	TM simulation time (hrs)
M1	34
M2	66
M3	20
M4	33
M5	51
M6	51
M7	171

# 6 Conclusion

## 6.1 Conclusion

The simulation results show us that the inherent strain method is a viable alternative method of simulation to replace the computationally costly TM simulation. The inherent strain method of simulation significantly reduces the computational time from a few days to a few hours. The simulation results of different subscale models have shown a systematic approach to setup the subscale model representing the large scale model.

The geometric properties of the subscale models were modified from a simple model to a more featured model which significantly increases the accuracy of the results. The deposition layers has less significance in the calibration process. Increasing the deposition layers does not increase the accuracy of the calibration process, except for the calibration of the last layer. Having 10 deposition layer model for simulation reduces the computational time by 41%.

The investigation on the influence of geometric properties of the subscale model shows that the more featured subscale models' inherent strain tensors were accurate when compared to the simple subscale model. Thus it is important to represent that the subscale model posses similar geometric properties of the large scale model.

The thermal BC has a significant impact on the accuracy of the calibration results as modeling with a realistic BC increases the accuracy of the calibration results.

The simulation results states that the inherent methodology minimizes the need for the computational costly TM simulation and reduces the computation time approximately by 85%. The inherent strain method is a viable alternative which can be used to ensure the manufacturability and quality of the product, at a earlier stage of the product development. Faster and accurate way of predicting of deformation and stresses, reduces the AM product development cycle.

## 6.2 Future Work

The future work should focus on minimizing the simulation time and improve the accuracy of the results. There are couple of things that can be investigated. Some of these are:

- A more featured subscale model involving the circular properties of the fan case can be modeled and analysed.
- Detailed analysis of the thermal BC2 can be carried out since the new thermal BC2 increases the accuracy of the calibration results.
- Investigate the thermal BC2 on a more featured model like M6 or M7 to verify the accuracy of the calibration results.
- Automizing a script for application of the thermal boundary condition. Since it is a time-consuming process. Because the thermal boundary condition is applied in a layer-wise manner.
- The Auto setup for AM simulation in MSC. Marc needs to be updated w.r.t to the new process parameters and simulation setup.



## References

- Bo Cheng, S. S. (2016). Stress and deformation evaluations of scanning strategy effect in selective laser melting. *Additive Manufacturing*, 240-251.
- CESEduPack. (2019). CES EduPack software, Granta Design Limited, Cambridge, UK, 2019.
- Donghong Ding, Z. P. (2015). Wire-feed additive manufacturing of metal components: technologies, developments and future interests. *The International Journal Of Advanced Manufacturing Technology*, 465-481.
- Forslund, V. (2018). *Using Cyclic Symmetry to Simplify Simulations in Additive Manufacturing*. Luleå, : Luleå University of Technology.
- Hryha, E. (2019). Lecture in MTT120 Additive Manufacturing: Overview of AM technologies and materials. Göteborg: Chalmers University of Technology.
- Iñaki Setien, M. C. (2019). Empirical methodology to determine inherent strains in additive manufacturing. *Computers and Mathematics with Applications*, 2282-2295.
- Lundbäck, A. (2010). *Modelling and Simulation of Welding and Metal Deposition*. LULEÅ : Luleå University of Technology.
- M. G. Yuan, Y. U. (1996). Prediction of Residual Stresses in Welded T- and I-Joints Using Inherent Strains. *Journal Of Engineering Materials And Technology*, 229-234.
- Matteo Bugatti, Q. S. (2018). Limitations of the inherent strain method in simulating powder bed fusion processes. *Additive Manufacturing*, 329-346.
- Mattsson, J. L. (2015). *Simplifications of Simulations in Additive Manufacturing Wire Feed Additive Manufacturing on Thin Structures*. LULEÅ : Luleå University of Technology.
- Michael Gouge, E. D. (2019). Experimental validation of thermo-mechanical part-scale modeling for laser powder bed fusion processes. *Additive Manufacturing*.
- Nils Keller, V. P. (2014). New method for fast predictions of residual stress and distortion of AM parts.
- Ploshikhin, V. P. (2010). Advanced numerical method for fast prediction of welding distortions of large aircraft structures. *International Journal Of Microstructure And Materials Properties*.
- Qian Chena, X. L. (2019). An inherent strain based multiscale modeling framework for simulating part-scale residual deformation for direct metal laser sintering. *Additive Manufacturing*, 406-418.
- Qingcheng Yang1, P. Z. (2016). Finite element modeling and validation of thermomechanical behavior of Ti-6Al-4V in directed energy deposition additive manufacturing. *Additive Manufacturing*, 169-177.
- Scott M. Thompsona, L. B. (2015). An overview of Direct Laser Deposition for additive manufacturing; Part I: Transport phenomena, modeling and diagnostics. *Additive Manufacturing*, 36-62.
- Sonja Jonsson, S. K. (2018). *Evaluation of residual stresses and distortions in additively manufactured components*. Stockholm: KTH Royal Institute Of Technology.

Xuan Liang, L. C. (2018). A modified method for estimating inherent strains from detailed process simulation for fast residual distortion prediction of single-walled structures fabricated by directed energy deposition. *Additive Manufacturing*, 471-486.

Xuan Liang, Q. C. (2019). Modified inherent strain method for efficient prediction of residual deformation in direct metal laser sintered components. *Computational Mechanics*, 1719–1733.

